ARTICLE

Experimental validation of unique combination numbers for third- and fourth-order neutron correlation factors of zero-power reactor noise

Tomohiro Endo[a*], Akio Yamamoto[a], Masao Yamanaka[b], Cheol Ho Pyeon[b]

[a] *Graduate School of Engineering, Nagoya University, Furo-cho, Chikusa-ku, Nagoya 464-8603, Japan;*

[b] *Division of Nuclear Engineering Science, Institute for Integrated Radiation and Nuclear Science, Kyoto University, Asashiro-nishi, Kumatori-cho, Sennan-gun, Osaka 590-0494, Japan*

Abstract

Zero-power reactor noise is useful for subcriticality measurements. Based on the nuclear reactor physics and the theory of neutron detection, this paper theoretically clarifies that the third- and fourth-order neutron correlation factors $\mathcal{Y}_3$ and $\mathcal{Y}_4$ can be expressed as functions of the second-order neutron correlation factor Y. In particular, if the neutron-counting gate width is sufficiently large, the saturation values $\mathcal{Y}_3/Y^2$ and $\mathcal{Y}_4/Y^3$ are almost equal to the unique combination numbers, '3' and '15,' for a source-driven subcritical system, where the subcriticality is less than 10000 pcm. These unique combination numbers, '3' and '15,' for $\mathcal{Y}_3/Y^2$ and $\mathcal{Y}_4/Y^3$ were validated using actual zero-power reactor noise measurements carried out at the Kyoto University Criticality Assembly. In this study, the estimation of statistical errors and correlations between different gate widths owing to the bunching method was achieved by the moving block bootstrap method. For a sufficiently long measured reactor noise in a steady and unperturbed state, a statistical test for the evaluation of the critical state and the absolute measurement of subcriticality can be carried out by statistically quantifying the difference between the measurement value of $\mathcal{Y}_3/Y^2$ and the unique combination number.

*Corresponding author. Email: t-endo@energy.nagoya-u.ac.jp

Keywords; reactor noise; Feynman-α method; higher-order neutron correlation; subcriticality; double factorial; bootstrap method; statistical error; covariance; KUCA; measurement

1. Introduction

Research on subcriticality measurement techniques is important to experimentally ensure criticality safety. Although various measurement techniques have been proposed and implemented, each technique presents both advantages and disadvantages. For example, for an unknown target system with a steady state, a dynamic technique such as the inverse kinetics method [1,2,3] is not applicable. A static technique such as the neutron source multiplication method [4,5,6] cannot be used to determine the absolute value of the effective neutron multiplication factor k_{eff} for the target system without additional information; *e.g.*, the neutron count rate for a reference state wherein k_{eff} is known, or the product of the detector efficiency and effective source strength. If there is no information on the presence of an external neutron source of which the strength cannot be neglected when compared with fission neutrons, the evaluation of the critical state is not simple using the conventional static technique, which focuses only on the average value of the neutron count rate in the target system.

In such a stationary unknown system, the measurement of the zero-power reactor noise (or the fluctuation of the neutron count around the average value) is useful to estimate the information related to the neutron multiplication [7]. The Feynman-α [8,9,10,11], Rossi-α [12,13], and power spectral density [14,15] methods are used as reactor noise analysis techniques, to measure the prompt neutron decay constant α that is expressed as $\alpha \approx (\beta_{\mathrm{eff}} - \rho)/\Lambda$ under a near-critical situation; where $-\rho \equiv (1 - k_{\mathrm{eff}})/k_{\mathrm{eff}}$, β_{eff}, and Λ are the subcriticality, effective delayed neutron fraction, and neutron generation time, respectively. For example, in the Feynman-α method, the time-series data of neutron counts are first measured. The second-order neutron correlation factor Y is then evaluated from the variance-to-mean ratio of the neutron counts, followed by the fitting procedure for the estimation of α. It should be noted that the point kinetics parameters β_{eff} and Λ or the prompt neutron decay constant at the critical state ($\alpha_{\mathrm{crit}} = \beta_{\mathrm{eff}}/\Lambda$) are required for the conversion from the measurement value of α to the subcriticality $-\rho$.

Accordingly, in previous research, it was suggested that the third-order neutron correlation factor $\mathcal{Y}_3$ contains useful information for the determination of the absolute value of the subcriticality $-\rho$ [16,17,18]. However, few reports are available on the experimental studies conducted on the higher-order neutron correlation factor [19,20]. One of the reasons for this is that the precise measurement of the higher-order neutron correlation factor is difficult, because the total measurement time of an experimental facility is limited. Moreover, an estimation technique for the statistical error of the higher-order neutron correlation factor was not sufficiently established in previous studies.

In recent studies, a technique using the bootstrap method [21,22] to estimate the statistical error of the second-order neutron correlation factor Y was proposed [10,11]. The estimated statistical error of Y was validated using the actual reactor noise measurement carried out at the Kyoto University Critical Assembly (KUCA). This statistical error estimation technique based on the bootstrap method can be also applied to the analog Monte Carlo simulation for the reactor noise measurement [23].

The aim of this study was to extend the applicability of the bootstrap method, for the practical estimation of the statistical errors of the third- and fourth-order neutron correlation factors ($\mathcal{Y}_3$ and $\mathcal{Y}_4$), in addition to the covariance matrices between different neutron-counting gate widths. Furthermore, by analyzing the reactor noise measurement carried out at the KUCA, the fundamental physical properties of the third- and fourth-order neutron correlation factors in the source-driven subcritical system were clarified. In particular, the primary aim was the demonstration of the following relationships in the case wherein the neutron-counting gate width T is sufficiently large under a relatively near-critical situation: $\mathcal{Y}_3/Y^2 \approx 3$ and $\mathcal{Y}_4/Y^3 \approx 15$. As described in the later section, the specific numbers of '3' and '15' are referred to as 'unique combination numbers' in this paper.

The remainder of the paper is structured as follows. In Section 2, a theory of the higher-order neutron correlation factors is presented. In Section 3, an explanation of the bootstrap method for the efficient estimation of statistical errors and correlations (covariance matrices) of the higher-order neutron correlation factors is presented. Section 4 presents a simple numerical simulation of the reactor noise for a non-multiplication system with a stationary external neutron source, to better characterize the property of the reactor noise in the non-multiplication system. In Section 5, the unique combination numbers of $\mathcal{Y}_3/Y^2$ and $\mathcal{Y}_4/Y^3$ are discussed with respect to an experimental analysis conducted on the actual zero-power reactor noise data that were measured at the KUCA. Section 6 notes the focus of future work, followed by the concluding remarks in Section 7.

2. Theory

2.1. Higher-order neutron correlation factors

Under the assumption that neutron counts $C(T)$ are detected within a counting gate width T for a steady state of a source-driven subcritical system, the nth-order neutron correlation factor $\mathcal{Y}_n(T)$ is defined as follows $(n \geq 2)$:

$$\mathcal{Y}_n(T) \equiv \frac{1}{\langle C(T) \rangle} \frac{\partial^n}{\partial Z^n} \ln\big(G(Z,T)\big)\Big|_{Z=1} , \tag{1}$$

$$G(Z,T) \equiv \sum_{C=0}^{\infty} Z^C P(C,T) , \tag{2}$$

where $P(C,T)$ is the probability that C neutrons are detected during the counting gate width T owing to the stationary external neutron source; $G(Z,T)$ is the probability generating function for $P(C,T)$; and the brackets $\langle\,\rangle$ indicate the expected value. For example, based on Equation (1), the second-, third-, and fourth-order neutron correlation factors ($Y(T)$, $\mathcal{Y}_3(T)$, and $\mathcal{Y}_4(T)$) can be evaluated as

$$Y(T) \equiv \mathcal{Y}_2(T) \equiv \frac{\kappa_2(T)}{\mu(T)} - 1 , \tag{3}$$

$$\mathcal{Y}_3(T) \equiv \frac{\kappa_3(T)}{\mu(T)} - 3\frac{\kappa_2(T)}{\mu(T)} + 2 = \left(\frac{\kappa_3(T)}{\mu(T)} - 1\right) - 3\left(\frac{\kappa_2(T)}{\mu(T)} - 1\right), \tag{4}$$

$$\begin{aligned}\mathcal{Y}_4(T) &\equiv \frac{\kappa_4(T)}{\mu(T)} - 6\frac{\kappa_3(T)}{\mu(T)} + 11\frac{\kappa_2(T)}{\mu(T)} - 6 \\ &= \left(\frac{\kappa_4(T)}{\mu(T)} - 1\right) - 6\left(\frac{\kappa_3(T)}{\mu(T)} - 1\right) + 11\left(\frac{\kappa_2(T)}{\mu(T)} - 1\right),\end{aligned} \tag{5}$$

where $\mu(T)$, $\kappa_2(T)$, $\kappa_3(T)$, and $\kappa_4(T)$ are the mean, and the second-, third-, and fourth-order cumulants, which are respectively defined as

$$\mu(T) \equiv \langle C(T) \rangle, \tag{6}$$

$$\kappa_2(T) \equiv \langle \left(C(T) - \mu(T)\right)^2 \rangle, \tag{7}$$

$$\kappa_3(T) \equiv \langle \left(C(T) - \mu(T)\right)^3 \rangle, \tag{8}$$

$$\kappa_4(T) \equiv \langle \left(C(T) - \mu(T)\right)^4 \rangle - 3\left(\kappa_2(T)\right)^2. \tag{9}$$

It should be noted that $\kappa_2(T)$ is identical to the variance, and $\kappa_3(T)$ and $\kappa_4(T)$ correspond to the skewness and kurtosis, respectively. If the probability distribution of $C(T)$ follows a Poisson distribution, $\mu(T) = \kappa_2(T) = \kappa_3(T) = \kappa_4(T)$. Therefore, $Y(T)$, $\mathcal{Y}_3(T)$, and $\mathcal{Y}_4(T)$ represent measures of the relative deviation from the Poisson distribution.

In an actual reactor noise measurement, the total measurement time is limited; therefore, the total number of samples for $C(T)$ is also finite. To reduce the bias for the limited number of neutron count data [24], the unbiased estimators $k_2(T)$, $k_3(T)$, and $k_4(T)$ are used for the experimental analysis of $\kappa_2(T)$, $\kappa_3(T)$, and $\kappa_4(T)$ [25]:

$$C_{\text{ave}}(T) = \frac{1}{N}\sum_{i=1}^{N} C_i(T), \tag{10}$$

$$k_2(T) = \frac{1}{N-1}\sum_{i=1}^{N}\left(C_i(T) - C_{\text{ave}}(T)\right)^2, \tag{11}$$

$$k_3(T) = \frac{N}{(N-1)(N-2)} \sum_{i=1}^{N} \left(C_i(T) - C_{\mathrm{ave}}(T) \right)^3 , \tag{12}$$

$$\begin{aligned} k_4(T) = {} & \frac{N(N+1)}{(N-1)(N-2)(N-3)} \sum_{i=1}^{N} \left(C_i(T) - C_{\mathrm{ave}}(T) \right)^4 \\ & - \frac{3}{(N-2)(N-3)} \left(\sum_{i=1}^{N} \left(C_i(T) - C_{\mathrm{ave}}(T) \right)^2 \right)^2 . \end{aligned} \tag{13}$$

Consequently, the neutron correlation factors are experimentally estimated as:

$$Y(T) = \frac{k_2(T)}{C_{\mathrm{ave}}(T)} - 1 , \tag{14}$$

$$\mathcal{Y}_3(T) = \frac{k_3(T)}{C_{\mathrm{ave}}(T)} - 3 \frac{k_2(T)}{C_{\mathrm{ave}}(T)} + 2 , \tag{15}$$

$$\mathcal{Y}_4(T) = \frac{k_4(T)}{C_{\mathrm{ave}}(T)} - 6 \frac{k_3(T)}{C_{\mathrm{ave}}(T)} + 11 \frac{k_2(T)}{C_{\mathrm{ave}}(T)} - 6. \tag{16}$$

2.2. Saturation values for $\boldsymbol{Y(T)}$, $\boldsymbol{\mathcal{Y}_3(T)}$, and $\boldsymbol{\mathcal{Y}_4(T)}$

As reported in previous studies [11,26,27], analytical formulae for the neutron count rate R and saturation values of $Y(T)$, $\mathcal{Y}_3(T)$, and $\mathcal{Y}_4(T)$ in the limit of $T \to \infty$ can be derived using the first- to fourth-order detector importance functions, $I_1^\dagger(\vec{r}, E, \vec{\Omega})$–$I_4^\dagger(\vec{r}, E, \vec{\Omega})$:

$$R \equiv \frac{\langle C(T) \rangle}{T} = \int_V S(\vec{r}) \sum_{q=0}^{\infty} p_{\mathrm{s}}(q, \vec{r})\, q \bar{I}_{1,\mathrm{s}}^\dagger(\vec{r}) dV , \tag{17}$$

$$\begin{aligned} & Y_\infty \equiv \lim_{T \to \infty} Y(T) \\ & = \frac{1}{R} \int_V S(\vec{r}) \sum_{q=0}^{\infty} p_{\mathrm{s}}(q, \vec{r}) \left(q \bar{I}_{2,\mathrm{s}}^\dagger(\vec{r}) + q(q-1) \left(\bar{I}_{1,\mathrm{s}}^\dagger(\vec{r}) \right)^2 \right) dV , \end{aligned} \tag{18}$$

$$\mathcal{Y}_{3,\infty} \equiv \lim_{T\to\infty} \mathcal{Y}_3(T)$$

$$= \frac{1}{R}\int_V \ S(\vec{r}) \sum_{q=0}^{\infty} p_{\mathrm{s}}(q,\vec{r}) \begin{pmatrix} q\bar{I}^{\dagger}_{3,\mathrm{s}}(\vec{r}) \\ +3q(q-1)\bar{I}^{\dagger}_{1,\mathrm{s}}(\vec{r})\bar{I}^{\dagger}_{2,\mathrm{s}}(\vec{r}) \\ +q(q-1)(q-2)\left(\bar{I}^{\dagger}_{1,\mathrm{s}}(\vec{r})\right)^3 \end{pmatrix} dV\,, \tag{19}$$

$$\mathcal{Y}_{4,\infty} \equiv \lim_{T\to\infty} \mathcal{Y}_4(T)$$

$$= \frac{1}{R}\int_V \ S(\vec{r}) \sum_{q=0}^{\infty} p_{\mathrm{s}}(q,\vec{r}) \begin{pmatrix} q\bar{I}^{\dagger}_{4,\mathrm{s}}(\vec{r}) \\ +4q(q-1)\bar{I}^{\dagger}_{1,\mathrm{s}}(\vec{r})\bar{I}^{\dagger}_{3,\mathrm{s}}(\vec{r}) \\ +3q(q-1)\left(\bar{I}^{\dagger}_{2,\mathrm{s}}(\vec{r})\right)^2 \\ +6q(q-1)(q-2)\left(\bar{I}^{\dagger}_{1,\mathrm{s}}(\vec{r})\right)^2 \bar{I}^{\dagger}_{2,\mathrm{s}}(\vec{r}) \\ +q(q-1)(q-2)(q-3)\left(\bar{I}^{\dagger}_{1,\mathrm{s}}(\vec{r})\right)^4 \end{pmatrix} dV\,, \tag{20}$$

$$\bar{I}^{\dagger}_{n,s}(\vec{r}) \equiv \int_0^{\infty} dE' \int_{4\pi} d\Omega' \frac{\chi_{\mathrm{s}}(\vec{r},E')}{4\pi} I^{\dagger}_n\left(\vec{r},E',\vec{\Omega}'\right), \tag{21}$$

where the subscript '∞' indicates the saturation values in the limit of $T \to \infty$; $S(\vec{r})$ is the spatial distribution of the source strength for the external neutron source; $\chi_{\mathrm{s}}(\vec{r},E)$ is the energy spectrum of the external neutron source; $p_{\mathrm{s}}(q,\vec{r})$ is the probability that q neutrons are emitted per decay of the external source; and $\bar{I}^{\dagger}_{n,\mathrm{s}}(\vec{r})$ is the weighted mean of the nth-order detector importance function $I^{\dagger}_n\left(\vec{r},E,\vec{\Omega}\right)$, which satisfies the following adjoint neutron transport equations [11,26,27]:

$$(\mathbf{A}^{\dagger} - \mathbf{F}^{\dagger})I^{\dagger}_1\left(\vec{r},E,\vec{\Omega}\right) = \Sigma_{\mathrm{d}}(\vec{r},E), \tag{22}$$

$$(\mathbf{A}^{\dagger} - \mathbf{F}^{\dagger})I^{\dagger}_2\left(\vec{r},E,\vec{\Omega}\right) = \Sigma_{\mathrm{f}}(\vec{r},E) \sum_{\nu=0}^{\infty} p_{\mathrm{f}}(\nu,\vec{r})\,\nu(\nu-1)\left(\bar{I}^{\dagger}_{1,\mathrm{f}}(\vec{r})\right)^2, \tag{23}$$

$$(\mathbf{A}^{\dagger} - \mathbf{F}^{\dagger})I^{\dagger}_3\left(\vec{r},E,\vec{\Omega}\right)$$

$$= \Sigma_{\mathrm{f}}(\vec{r},E) \sum_{\nu=0}^{\infty} p_{\mathrm{f}}(\nu,\vec{r}) \begin{pmatrix} 3\nu(\nu-1)\bar{I}^{\dagger}_{1,\mathrm{f}}(\vec{r})\bar{I}^{\dagger}_{2,\mathrm{f}}(\vec{r}) \\ +\nu(\nu-1)(\nu-2)\left(\bar{I}^{\dagger}_{1,\mathrm{f}}(\vec{r})\right)^3 \end{pmatrix}, \tag{24}$$

$$
\begin{aligned}
&(\mathbf{A}^{\dagger}-\mathbf{F}^{\dagger}) I_4^{\dagger}(\vec{r}, E, \vec{\Omega}) \\
&= \Sigma_{\mathrm{f}}(\vec{r}, E) \sum_{\nu=0}^{\infty} p_{\mathrm{f}}(\nu, \vec{r}) \begin{pmatrix} 4\nu(\nu-1) \bar{I}_{1,\mathrm{f}}^{\dagger}(\vec{r}) \bar{I}_{3,\mathrm{f}}^{\dagger}(\vec{r}) \\ +3\nu(\nu-1)\left(\bar{I}_{2,\mathrm{f}}^{\dagger}(\vec{r})\right)^2 \\ +6\nu(\nu-1)(\nu-2)\left(\bar{I}_{1,\mathrm{f}}^{\dagger}(\vec{r})\right)^2 \bar{I}_{2,\mathrm{f}}^{\dagger}(\vec{r}) \\ +\nu(\nu-1)(\nu-2)(\nu-3)\left(\bar{I}_{1,\mathrm{f}}^{\dagger}(\vec{r})\right)^4 \end{pmatrix},
\end{aligned} \tag{25}
$$

$$
\bar{I}_{n,\mathrm{f}}^{\dagger}(\vec{r}) \equiv \int_0^{\infty} dE' \int_{4\pi} d\Omega' \frac{\chi_{\mathrm{f}}(\vec{r}, E')}{4\pi} I_n^{\dagger}(\vec{r}, E', \vec{\Omega}'), \tag{26}
$$

$$
\mathbf{A}^{\dagger} \equiv -\vec{\Omega}\nabla + \Sigma_{\mathrm{t}}(\vec{r}, E) - \int_0^{\infty} dE' \int_{4\pi} d\Omega' \, \Sigma_{\mathrm{s}}(\vec{r}, E \to E', \vec{\Omega} \to \vec{\Omega}'), \tag{27}
$$

$$
\mathbf{F}^{\dagger} \equiv \nu\Sigma_{\mathrm{f}}(\vec{r}, E) \int_0^{\infty} dE' \int_{4\pi} d\Omega' \frac{\chi_{\mathrm{f}}(\vec{r}, E')}{4\pi}, \tag{28}
$$

where the superscript '†' indicates the adjoint; $\mathbf{A}^{\dagger}$ and $\mathbf{F}^{\dagger}$ are the adjoint net neutron loss, and neutron production operators, respectively; $\Sigma_{\mathrm{d}}(\vec{r}, E)$ is the macroscopic neutron detection cross-section; $\chi_{\mathrm{f}}(\vec{r}, E)$ is the energy spectrum of fission; $p_{\mathrm{f}}(\nu, \vec{r})$ is the probability that ν neutrons are emitted per fission; and the other notations maintain their conventional meanings in the nuclear reactor physics.

Under the assumption that the fundamental mode approximation is applicable, $I_n^{\dagger}(\vec{r}, E, \vec{\Omega})$ is expressed as

$$
I_n^{\dagger}(\vec{r}, E, \vec{\Omega}) \approx c_n \psi_0^{\dagger}(\vec{r}, E, \vec{\Omega}), \tag{29}
$$

where c_n is the expansion coefficient, and $\psi_0^{\dagger}(\vec{r}, E, \vec{\Omega})$ is the adjoint k_{eff}-eigenfunction that satisfies the following adjoint k_{eff}-eigenvalue equation:

$$
\mathbf{A}^{\dagger}\psi_0^{\dagger}(\vec{r}, E, \vec{\Omega}) = \frac{1}{k_{\mathrm{eff}}} \mathbf{F}^{\dagger}\psi_0^{\dagger}(\vec{r}, E, \vec{\Omega}). \tag{30}
$$

The fundamental mode approximation of Equation (29) is more reasonable under a subcritical condition, where the effective neutron multiplication factor k_{eff} is closer to unity. The expansion coefficient c_n can be theoretically obtained by multiplying Equations (22)–(25) by the forward k_{eff}-eigenfunction $\psi_0(\vec{r},E,\vec{\Omega})$ and by using the orthogonality condition between the forward and adjoint eigenfunctions. Here, the forward eigenfunction $\psi_0(\vec{r},E,\vec{\Omega})$ satisfies the following equation:

$$\mathbf{A}\psi_0(\vec{r},E,\vec{\Omega}) = \frac{1}{k_{\mathrm{eff}}}\mathbf{F}\psi_0(\vec{r},E,\vec{\Omega}), \tag{31}$$

$$\mathbf{A} \equiv \vec{\Omega}\nabla + \Sigma_{\mathrm{t}}(\vec{r},E) - \int_0^\infty dE' \int_{4\pi} d\Omega'\, \Sigma_{\mathrm{s}}(\vec{r},E' \to E,\vec{\Omega}' \to \vec{\Omega}), \tag{32}$$

$$\mathbf{F} \equiv \frac{\chi_{\mathrm{f}}(\vec{r},E)}{4\pi}\int_0^\infty dE' \int_{4\pi} d\Omega'\, \nu\Sigma_{\mathrm{f}}(\vec{r},E'); \tag{33}$$

and the orthogonality condition of the eigenfunctions can be expressed as follows:

$$\int_V dV \int_0^\infty dE \int_{4\pi} d\Omega \left(\psi_0(\vec{r},E,\vec{\Omega})\mathbf{F}^\dagger\psi_m^\dagger(\vec{r},E',\vec{\Omega}')\right) = \mathcal{F}_1\delta_{0,m}, \tag{34}$$

where $\psi_m^\dagger(\vec{r},E,\vec{\Omega})$ is the mth-order adjoint eigenfunction; $\delta_{0,m}$ is the Kronecker delta; and the parameter $\mathcal{F}_n$ is conveniently introduced using the scalar flux ϕ_0 and the fission-source-averaged value for $\psi_0^\dagger$, as follows:

$$\mathcal{F}_n \equiv \int_V dV \int_0^\infty dE\, \Sigma_{\mathrm{f}}(\vec{r},E)\phi_0(\vec{r},E) \sum_{\nu=0}^{\infty} \frac{\nu!}{(\nu-n)!} p_{\mathrm{f}}(\nu,\vec{r},E) \left(\bar{\psi}_{0,\mathrm{f}}^\dagger(\vec{r})\right)^n, \tag{35}$$

$$\phi_0(\vec{r},E) \equiv \int_{4\pi} \psi_0(\vec{r},E,\vec{\Omega}')d\Omega', \tag{36}$$

$$\bar{\psi}_{0,\mathrm{f}}^\dagger(\vec{r}) \equiv \int_0^\infty dE' \int_{4\pi} d\Omega' \frac{\chi_{\mathrm{f}}(\vec{r},E')}{4\pi}\psi_0^\dagger(\vec{r},E',\vec{\Omega}'). \tag{37}$$

Consequently, $I_n^\dagger(\vec{r},E,\vec{\Omega})$ can be approximated as follows:

$$I_1^\dagger(\vec{r},E,\vec{\Omega}) \approx \frac{\mathcal{D}}{-\rho\mathcal{F}_1}\psi_0^\dagger(\vec{r},E,\vec{\Omega}), \tag{38}$$

$$I_2^\dagger(\vec{r},E,\vec{\Omega}) \approx \left(\frac{\mathcal{D}}{-\rho\mathcal{F}_1}\right)^2 \frac{\mathcal{F}_2}{-\rho\mathcal{F}_1}\psi_0^\dagger(\vec{r},E,\vec{\Omega}), \tag{39}$$

$$I_3^{\dagger}(\vec{r},E,\vec{\Omega}) \approx \left(\frac{\mathcal{D}}{-\rho\mathcal{F}_1}\right)^3 \left(3\left(\frac{\mathcal{F}_2}{-\rho\mathcal{F}_1}\right)^2 + \frac{\mathcal{F}_3}{-\rho\mathcal{F}_1}\right)\psi_0^{\dagger}(\vec{r},E,\vec{\Omega}), \tag{40}$$

$$I_4^{\dagger}(\vec{r},E,\vec{\Omega}) \approx \left(\frac{\mathcal{D}}{-\rho\mathcal{F}_1}\right)^4 \left(15\left(\frac{\mathcal{F}_2}{-\rho\mathcal{F}_1}\right)^3 + 10\frac{\mathcal{F}_2\mathcal{F}_3}{(-\rho\mathcal{F}_1)^2} + \frac{\mathcal{F}_4}{-\rho\mathcal{F}_1}\right)\psi_0^{\dagger}(\vec{r},E,\vec{\Omega}), \tag{41}$$

$$\mathcal{D} \equiv \int_V dV \int_0^{\infty} dE\, \Sigma_{\mathrm{d}}(\vec{r},E)\phi_0(\vec{r},E), \tag{42}$$

where the parameter $\mathcal{D}$ is introduced for convenience and $\mathcal{D}/\mathcal{F}_1$ corresponds to the detection efficiency.

By substituting Equations (38)–(41) into Equations (17)–(20), the saturation values based on the fundamental mode approximation can be re-written as follows:

$$Y_{\infty} \approx \left(\frac{\mathcal{D}}{-\rho\mathcal{F}_1}\right)\left(\frac{\mathcal{F}_2}{-\rho\mathcal{F}_1} + \frac{\mathcal{S}_2}{\mathcal{S}_1}\right), \tag{43}$$

$$\mathcal{Y}_{3,\infty} \approx \left(\frac{\mathcal{D}}{-\rho\mathcal{F}_1}\right)^2 \left(\frac{\mathcal{F}_3}{-\rho\mathcal{F}_1} + \frac{\mathcal{S}_3}{\mathcal{S}_1} + 3\frac{\mathcal{F}_2}{-\rho\mathcal{F}_1}\left(\frac{\mathcal{F}_2}{-\rho\mathcal{F}_1} + \frac{\mathcal{S}_2}{\mathcal{S}_1}\right)\right), \tag{44}$$

$$\mathcal{Y}_{4,\infty} \approx \left(\frac{\mathcal{D}}{-\rho\mathcal{F}_1}\right)^3 \left(\begin{array}{c} \frac{\mathcal{F}_4}{-\rho\mathcal{F}_1} + \frac{\mathcal{S}_4}{\mathcal{S}_1} + 6\frac{\mathcal{F}_2}{-\rho\mathcal{F}_1}\left(\frac{\mathcal{F}_3}{-\rho\mathcal{F}_1} + \frac{\mathcal{S}_3}{\mathcal{S}_1}\right) \\ + \left(4\frac{\mathcal{F}_3}{-\rho\mathcal{F}_1} + 15\left(\frac{\mathcal{F}_2}{-\rho\mathcal{F}_1}\right)^2\right)\left(\frac{\mathcal{F}_2}{-\rho\mathcal{F}_1} + \frac{\mathcal{S}_2}{\mathcal{S}_1}\right) \end{array}\right), \tag{45}$$

$$\mathcal{S}_n \equiv \int_V dV\, S(\vec{r}) \sum_{q=0}^{\infty} \frac{q!}{(q-n)!} p_{\mathrm{s}}(q,\vec{r}) \left(\bar{\psi}_{0,\mathrm{s}}^{\dagger}(\vec{r})\right)^n, \tag{46}$$

$$\bar{\psi}_{0,\mathrm{s}}^{\dagger}(\vec{r}) \equiv \int_0^{\infty} dE' \int_{4\pi} d\Omega' \frac{\chi_{\mathrm{s}}(\vec{r},E')}{4\pi} \psi_0^{\dagger}(\vec{r},E',\vec{\Omega}'). \tag{47}$$

From Equations (43)–(45), if $-\rho < 0.1$ (*dk/k*) (or $0.9 < k_{\mathrm{eff}} < 1$), the ratios of $\mathcal{Y}_{3,\infty}/Y_{\infty}^2$ and $\mathcal{Y}_{4,\infty}/Y_{\infty}^3$ can be further approximated by linear functions with respect to $-\rho$:

$$\frac{\mathcal{Y}_{3,\infty}}{Y_{\infty}^2} \approx 3 + \frac{\mathcal{F}_1}{\mathcal{F}_2}\left(\frac{\mathcal{F}_3}{\mathcal{F}_2} - 3\frac{\mathcal{S}_2}{\mathcal{S}_1}\right)(-\rho), \tag{48}$$

$$\frac{\mathcal{Y}_{4,\infty}}{Y_\infty^3} \approx 15 + 10\frac{\mathcal{F}_1}{\mathcal{F}_2}\left(\frac{\mathcal{F}_3}{\mathcal{F}_2} - 3\frac{\mathcal{S}_2}{\mathcal{S}_1}\right)(-\rho), \tag{49}$$

where the magnitude of $\left|\frac{\mathcal{F}_1}{\mathcal{F}_2}\left(\frac{\mathcal{F}_3}{\mathcal{F}_2} - 3\frac{\mathcal{S}_2}{\mathcal{S}_1}\right)\right|$ is approximately 1 [18,28]. For a simple example, in the case of an infinite homogeneous system of ^{235}U with a Poisson source ($\langle q(q-1)\rangle = 0$), $\left|\frac{\mathcal{F}_1}{\mathcal{F}_2}\left(\frac{\mathcal{F}_3}{\mathcal{F}_2} - 3\frac{\mathcal{S}_2}{\mathcal{S}_1}\right)\right| = \frac{\langle\nu\rangle\langle\nu(\nu-1)(\nu-2)\rangle}{\langle\nu(\nu-1)\rangle^2} \approx 0.8$. As k_{eff} approaches unity (or $-\rho \to +0$), $\mathcal{Y}_{3,\infty}/Y_\infty^2$ and $\mathcal{Y}_{4,\infty}/Y_\infty^3$ converge to the constant values independent of $\mathcal{F}_n$ and $\mathcal{S}_n$:

$$\lim_{-\rho\to+0}\frac{\mathcal{Y}_{3,\infty}}{Y_\infty^2} \approx 3, \tag{50}$$

$$\lim_{-\rho\to+0}\frac{\mathcal{Y}_{4,\infty}}{Y_\infty^3} \approx 15. \tag{51}$$

As shown in Figure 1, the unique combination numbers, ‘3’ and ‘15,’ correspond to the total number of combinations for the trio- and quartet-detections that have two and three two-forked branches, respectively.

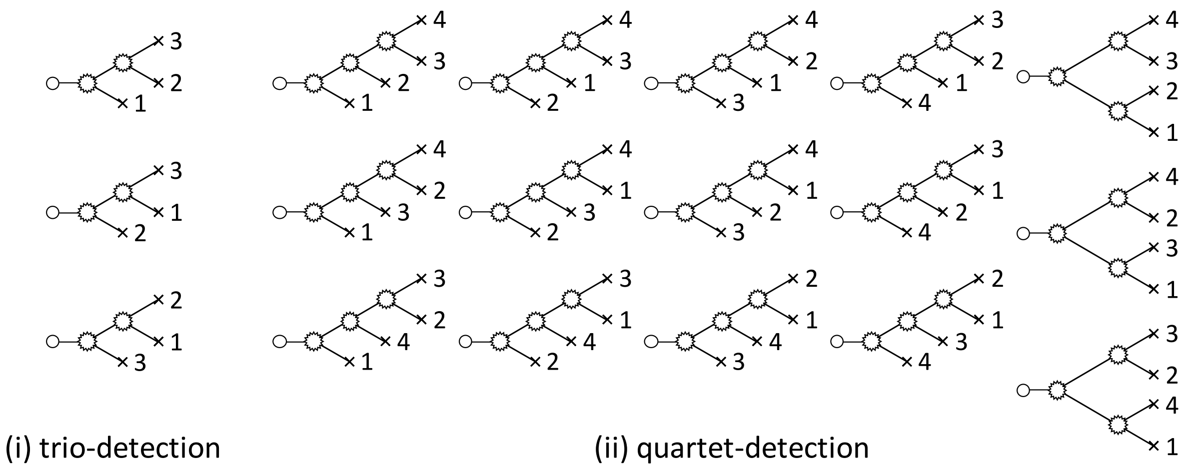

Figure 1 Combinations for trio- and quartet-detections

On the contrary, in the limit of $k_{\mathrm{eff}} \to +0$ or $-\rho \to +\infty$, the higher-order importance functions $I_2^\dagger(\vec{r}, E, \vec{\Omega})$–$I_4^\dagger(\vec{r}, E, \vec{\Omega})$ are zero, because $\Sigma_{\mathrm{f}}(\vec{r}, E) = 0$ in Equations (23)–(25). Consequently, the ratios of $\mathcal{Y}_{3,\infty}/Y_\infty^2$ and $\mathcal{Y}_{4,\infty}/Y_\infty^3$ converge to particular values that are dependent on the multiplicity of the external neutron source:

$$\lim_{-\rho\to+\infty}\frac{\mathcal{Y}_{3,\infty}}{Y_{\infty}^{2}}=\frac{\left(\begin{array}{c}\left(\int_V S(\vec{r})\sum_{q=0}^{\infty}p_{\mathrm{s}}(q,\vec{r})\,q\bar{I}_{1,\mathrm{s}}^{\dagger}(\vec{r})dV\right)\times\\ \left(\int_V S(\vec{r})\sum_{q=0}^{\infty}p_{\mathrm{s}}(q,\vec{r})\,q(q-1)(q-2)\left(\bar{I}_{1,\mathrm{s}}^{\dagger}(\vec{r})\right)^{3}dV\right)\end{array}\right)}{\left(\int_V S(\vec{r})\sum_{q=0}^{\infty}p_{\mathrm{s}}(q,\vec{r})\,q(q-1)\left(\bar{I}_{1,\mathrm{s}}^{\dagger}(\vec{r})\right)^{2}dV\right)^{2}},\tag{52}$$

$$\lim_{-\rho\to+\infty}\frac{\mathcal{Y}_{4,\infty}}{Y_{\infty}^{3}}=\frac{\left(\begin{array}{c}\left(\int_V S(\vec{r})\sum_{q=0}^{\infty}p_{\mathrm{s}}(q,\vec{r})\,q\bar{I}_{1,\mathrm{s}}^{\dagger}(\vec{r})dV\right)^{2}\times\\ \left(\int_V S(\vec{r})\sum_{q=0}^{\infty}p_{\mathrm{s}}(q,\vec{r})\,q(q-1)(q-2)(q-3)\left(\bar{I}_{1,\mathrm{s}}^{\dagger}(\vec{r})\right)^{4}dV\right)\end{array}\right)}{\left(\int_V S(\vec{r})\sum_{q=0}^{\infty}p_{\mathrm{s}}(q,\vec{r})\,q(q-1)\left(\bar{I}_{1,\mathrm{s}}^{\dagger}(\vec{r})\right)^{2}dV\right)^{3}}.\tag{53}$$

If the external source $S(\vec{r})$ is a point-wise source of the Dirac delta function, Equations (52)–(53) are further simplified as follows:

$$\lim_{-\rho\to+\infty}\frac{\mathcal{Y}_{3,\infty}}{Y_{\infty}^{2}}\approx\frac{\langle q\rangle\langle q(q-1)(q-2)\rangle}{\langle q(q-1)\rangle^{2}},\tag{54}$$

$$\lim_{-\rho\to+\infty}\frac{\mathcal{Y}_{4,\infty}}{Y_{\infty}^{3}}\approx\frac{\langle q\rangle^{2}\langle q(q-1)(q-2)(q-3)\rangle}{\langle q(q-1)\rangle^{3}}.\tag{55}$$

For example, in the case of a spontaneous fission nuclide such as ^{252}Cf, $\frac{\langle q\rangle\langle q(q-1)(q-2)\rangle}{\langle q(q-1)\rangle^{2}}\approx 0.8$ and $\frac{\langle q\rangle^{2}\langle q(q-1)(q-2)(q-3)\rangle}{\langle q(q-1)\rangle^{3}}\approx 0.6$ [28], thus the ratios of $\mathcal{Y}_{3,\infty}/Y_{\infty}^{2}$ and $\mathcal{Y}_{4,\infty}/Y_{\infty}^{3}$ under the condition of $k_{\mathrm{eff}}=0$ are significantly different from the unique combination numbers, ‘3’ and ‘15,’ near the critical state.

3. Bootstrap method for statistical error estimation of $\mathcal{Y}_n$

In the previous study, the statistical error estimation for the Feynman-α method using the bootstrap method was proposed for the practical estimation of the statistical errors of both Y and the prompt neutron decay constant α [10]. Subsequently, the error estimation technique was improved to effectively calculate the covariance matrix of $Y(T)$ between different gate widths T [11]. This improvement was achieved using the recursive bunching method. In this study, the moving block bootstrap method [22] was used to estimate the statistical errors of the higher-order neutron correlation factors $\mathcal{Y}_n(T)$ and their covariance matrices. Details of the procedure are presented below:

1. The original time-series data of the neutron counts $\vec{C}(T_0) = \left[C_1, C_2, \cdots, C_{N_0}\right]$ are provided by a single measurement of the reactor noise, where the basic counting gate width is T_0, and the total number of count data is N_0.
2. An upper limit value of the bunching is set as M, where $1 < M < N_0$.
3. An empty vector $\vec{C}^*(T_0) = [\,]$ is prepared ($i = 1$).
4. The 'resampling position ξ_i' is determined using a uniform random integer number, $1 \leq \xi_i \leq (N_0 - M + 1)$. Successive time-series data $\vec{C}_{\xi_i} = \left[C_{\xi_i}, C_{\xi_i+1}, \cdots, C_{\xi_i+M-1}\right]$ are then extracted from the original time series data and added to the end of the vector $\vec{C}^*(T_0)$. This extraction of successive data is necessary for the estimate of the covariance matrices of the higher-order neutron correlation factors and the ratios.
5. As shown in Figure 2, a 'bootstrap sample of the time-series data $\vec{C}^*(T_0)$' is newly generated by repeating Step 4 L times:

$$\vec{C}^*(T_0) = [\vec{C}_{\xi_1}, \vec{C}_{\xi_2}, \cdots, \vec{C}_{\xi_L}], \tag{56}$$

where $L = \lceil N_0/M \rceil$. It should be noted that extra data in $\vec{C}_{\xi_L}$ is removed if necessary, so that the total number of count data in $\vec{C}^*(T_0)$ is N_0.

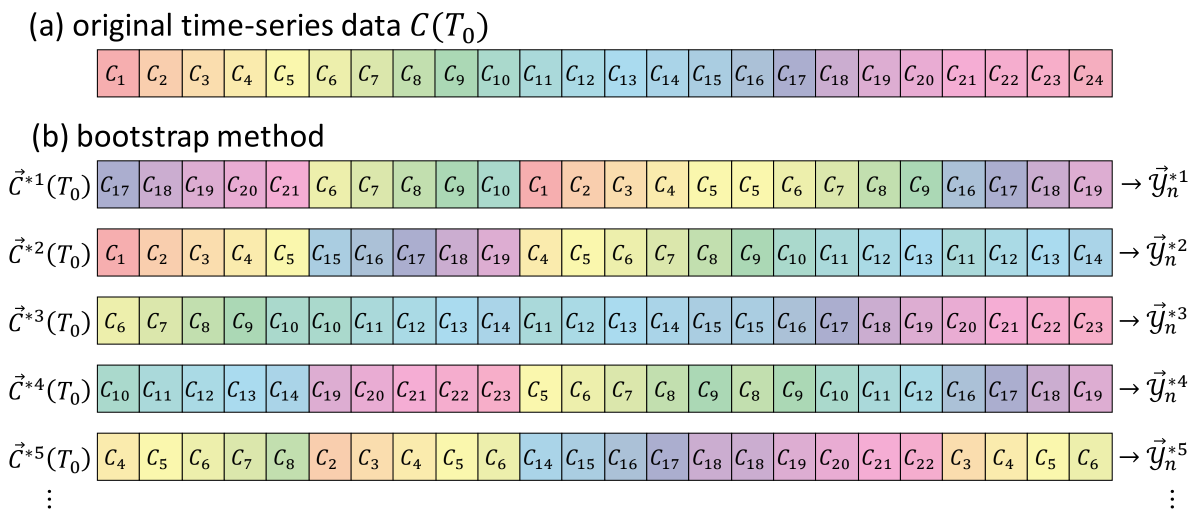

Figure 2 Example of the moving block bootstrap method ($N_0 = 24, M = 5$)

6. Using the recursive bunching method with Equations (10)–(16) for the bootstrap sample $\vec{C}^*(T_0)$ in Step 5, the variations in the 'bootstrap replicates $\mathcal{Y}_n^*(kT_0)$, $\frac{\mathcal{Y}_3^*(kT_0)}{(Y^*(kT_0))^2}$, and $\frac{\mathcal{Y}_4^*(kT_0)}{(Y^*(kT_0))^3}$' are evaluated for the bunching gate width kT_0, where k is the bunching number $(1 \le k \le M)$. As shown in Figure 3, the bunching method is recursively applied to previously-bunched data, *i.e.*, $\vec{C}^*(2kT_0)$ is effectively produced by combining a pair of successive elements in $\vec{C}^*(kT_0)$. Here, the bunching number k is given by $k = p \times 2^j$ $(j = 0,1,\cdots)$. For example, the initial bunching number p is empirically determined as $p = 2,3,5,7,9,11,13,15,17,19,21,23,25,27,29,31,$ and 33. The maximum value of j is limited to satisfy $p \times 2^j \le M$. Consequently, row vectors $\vec{\mathcal{Y}}_n^* = [\mathcal{Y}_n^*(T_0), \mathcal{Y}_n^*(2T_0), \cdots, \mathcal{Y}_n^*(MT_0)]$, $\vec{r}_3^* = \left[\frac{\mathcal{Y}_3^*(T_0)}{(Y^*(T_0))^2}, \frac{\mathcal{Y}_3^*(2T_0)}{(Y^*(2T_0))^2}, \cdots, \frac{\mathcal{Y}_3^*(MT_0)}{(Y^*(MT_0))^2}\right]$, and $\vec{r}_4^* = \left[\frac{\mathcal{Y}_4^*(T_0)}{(Y^*(T_0))^3}, \frac{\mathcal{Y}_4^*(2T_0)}{(Y^*(2T_0))^3}, \cdots, \frac{\mathcal{Y}_4^*(MT_0)}{(Y^*(MT_0))^3}\right]$ are obtained.

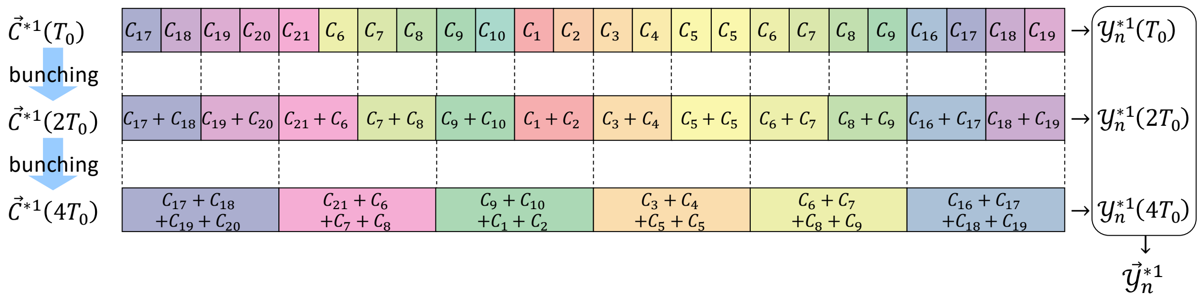

Figure 3 Example of the recursive bunching method ($p = 2$)

7. To estimate the confidence intervals and covariance matrices of $\vec{\mathcal{Y}}_n^*$, $\vec{r}_3^*$, and $\vec{r}_4^*$, Steps 3–6 are repeated B times. Consequently, a set of bootstrap replicates $\vec{\mathcal{Y}}_n^{*b}$, $\vec{r}_3^{*b}$, and $\vec{r}_4^{*b}$, are obtained for $b = 1,2,\cdots,B$, where B is the total number of bootstrap replicates.
8. As a result of Step 7, frequency distributions of $\mathcal{Y}_n^*(kT_0)$, $\frac{\mathcal{Y}_3^*(kT_0)}{(Y^*(kT_0))^2}$, and $\frac{\mathcal{Y}_4^*(kT_0)}{(Y^*(kT_0))^3}$ are obtained. On the basis of these 'bootstrap frequency distributions,' the percentile

confidence intervals (or 2.5 and 97.5 percentile points) can be simply estimated to evaluate the range of statistical errors of $\mathcal{Y}_n^*(kT_0)$, $\frac{\mathcal{Y}_3^*(kT_0)}{(Y^*(kT_0))^2}$, and $\frac{\mathcal{Y}_4^*(kT_0)}{(Y^*(kT_0))^3}$. For example, the B bootstrap replicates $\mathcal{Y}_n^{*b}(kT_0)$ are sorted in ascending order. The lower and upper limits of the 95% bootstrap confidence interval are simply estimated from the $(0.025 \times B)$th and $(0.975 \times B)$th smallest values of sorted $\mathcal{Y}_n^{*b}(kT_0)$, respectively.

9. Using the row vectors $\vec{\mathcal{Y}}_n^{*b}$, $\vec{r}_3^{*b}$, and $\vec{r}_4^{*b}$, these bootstrap covariance matrices can be estimated, if necessary. For example, the covariance matrix $\mathbf{\Sigma}_{\mathcal{Y}_n^*}$ is calculated as follows:

$$\mathbf{\Sigma}_{\mathcal{Y}_n^*} = \frac{1}{B-1}\sum_{b=1}^{B}\left(\vec{\mathcal{Y}}_n^{*b} - \vec{\mathcal{Y}}_{\mathrm{ave}}^*\right)^T\left(\vec{\mathcal{Y}}_n^{*b} - \vec{\mathcal{Y}}_{\mathrm{ave}}^*\right), \tag{57}$$

$$\vec{\mathcal{Y}}_{\mathrm{ave}}^* = \frac{1}{B}\sum_{b=1}^{B}\vec{\mathcal{Y}}_n^{*b}, \tag{58}$$

where the superscript T indicates the transpose. In the same manner as presented in Equation (57), the covariance matrices $\mathbf{\Sigma}_{r_3^*}$ and $\mathbf{\Sigma}_{r_4^*}$ can be also estimated using $\vec{r}_3^{*b}$ and $\vec{r}_4^{*b}$ instead of $\vec{\mathcal{Y}}_n^{*b}$, respectively.

4. Zero-power reactor noise simulation for non-multiplication system

4.1. Calculation conditions of numerical simulation

To understand the reactor noise in the non-multiplication system, a very simple Monte Carlo simulation was conducted in the same manner as in the previous studies [24,27]. If possible, the validation should be carried out using an actual reactor noise measurement. However, it is not easy to measure the statistically significant data for an actual non-multiplication system with an external neutron source such as a ^{252}Cf spontaneous source, given that the magnitude of neutron correlation factors $\mathcal{Y}_n$ are significantly small owing to the absence of fission chain reactions [29]. Thus, in future work, the validation will be conducted by carrying out actual measurements using a high-efficiency neutron detection system, which is beyond the scope of this study.

In the Monte Carlo simulation, an infinite homogenous system with a stationary external neutron source was assumed. In this study, the external neutron source was a spontaneous fission source of ^{252}Cf and the probability distribution of $p_s(q)$ was quoted from Reference [28]. Therefore, the factorial moments of q were calculated as follows: $\langle q\rangle = 3.77$, $\langle q(q-1)\rangle = 12.05$, $\langle q(q-1)(q-2)\rangle = 32.03$, and $\langle q(q-1)(q-2)(q-3)\rangle = 69.52$. The source strength S was set as $S = 100$ (neutrons/s). For simplicity, the neutron energy was one group, and all the absorbed neutrons were assumed to be detected to obtain the time-series data. The product of the neutron velocity and macroscopic absorption cross-section ($v\Sigma_a$) was set as $v\Sigma_a = 10000$ (1/s), which also corresponds to the prompt neutron decay constant α in this simple problem. The virtual measurement time of the reactor noise (N_0T_0) was 10000 (s).

Using the recursive bunching method for the simulated time-series data, the saturation values of $\frac{\mathcal{Y}_3(kT_0)}{\left(Y(kT_0)\right)^2}$ and $\frac{\mathcal{Y}_4(kT_0)}{\left(Y(kT_0)\right)^3}$ were numerically investigated using the methodology described in Section 3, where $T_0 = 2\times 10^{-5}$ (s), $M = 512$, and the total number of count data N_0 was 5×10^8. To estimate the statistical errors of $\frac{\mathcal{Y}_3(kT_0)}{\left(Y(kT_0)\right)^2}$ and $\frac{\mathcal{Y}_4(kT_0)}{\left(Y(kT_0)\right)^3}$, the 95% bootstrap confidence intervals were also calculated using the moving block bootstrap method with $B = 1000$.

4.2. Numerical results

Figure 4 presents numerical results of the ratios of $\frac{\mathcal{Y}_3(T)}{\left(Y(T)\right)^2}$ and $\frac{\mathcal{Y}_4(T)}{\left(Y(T)\right)^3}$, where the error bars indicate the 95% bootstrap confidence intervals. As T becomes sufficiently large, it was confirmed that these values converge to the saturation values. As can be expected with respect to Equations (54) and (55), the saturation values were approximately $\frac{\langle q\rangle\langle q(q-1)(q-2)\rangle}{\langle q(q-1)\rangle^2} = 0.832$ and $\frac{\langle q\rangle^2\langle q(q-1)(q-2)(q-3)\rangle}{\langle q(q-1)\rangle^3} = 0.566$, although the statistical errors tended to increase as T increased. The saturation values of $\frac{\mathcal{Y}_3(T)}{\left(Y(T)\right)^2}$ and $\frac{\mathcal{Y}_4(T)}{\left(Y(T)\right)^3}$ in the non-multiplication system were significantly different from the unique combination numbers, '3' and '15,' in the source-driven subcritical system. This implies that the detection of the neutron multiplication induced by fissile materials can be statistically evaluated from the differences between $\mathcal{Y}_{3,\infty}/Y_\infty^2$ and '3' and between $\mathcal{Y}_{4,\infty}/Y_\infty^3$ and '15.'

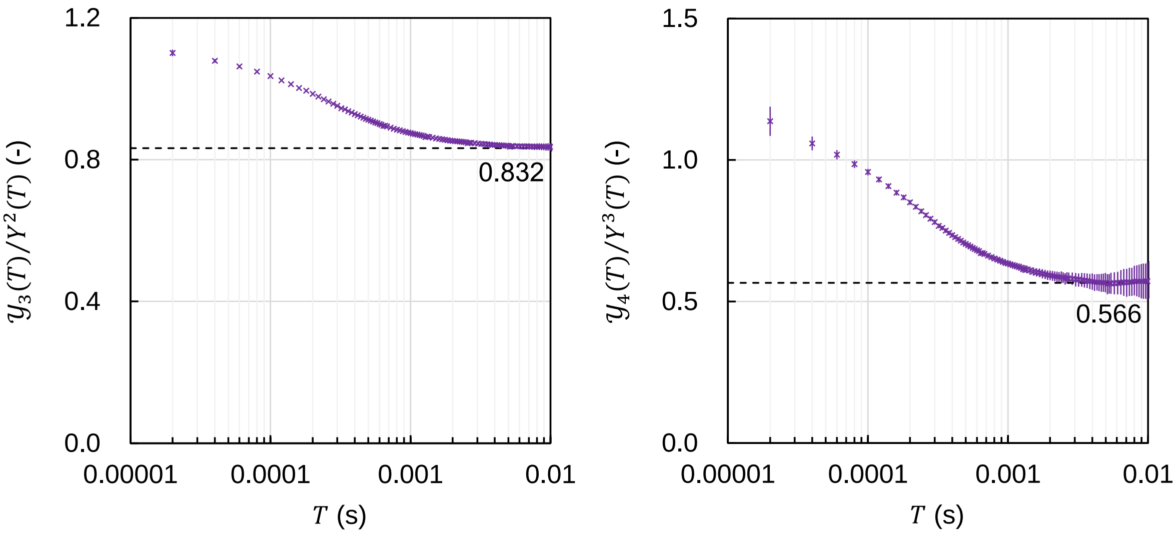

Figure 4 Numerical results of saturation values for $\boldsymbol{\mathcal{Y}_3(T)/\left(Y(T)\right)^2}$ and $\boldsymbol{\mathcal{Y}_4(T)/\left(Y(T)\right)^3}$ in the non-multiplication system with ^{252}Cf source

5. Zero-power reactor noise measurements for actual subcritical system

5.1. Experimental conditions

In the previous studies [10,11,30], several series of reactor noise experiments were conducted in the A-core (A3/8"p36EU-NU) at the KUCA. The experimental conditions are briefly explained below.

The experimental cores and the loaded fuel assemblies are presented in Figure 5 and Figure 6, respectively. The core-average ^{235}U enrichment was 5.4 wt%. In the experimental analysis, the following three cases were analyzed: (a) All control Rods In (ARI), (b) Shutdown, and (c) Shutdown with the replacement of fuel assemblies using Polyethylene reflectors (Shutdown+P). In Cases (b) and (c), 3×3 fuel and reflector assemblies were fully withdrawn, because the reactor is shutdown state. In Case (c), the three fuel assemblies were replaced by the polyethylene reflector assemblies to obtain the deeper subcriticality. For Cases (a)–(c), the numerical results of k_{eff}, β_{eff}, and Λ using MCNP6.2 [31] with JENDL-4.0 [32] are presented in Table 1.

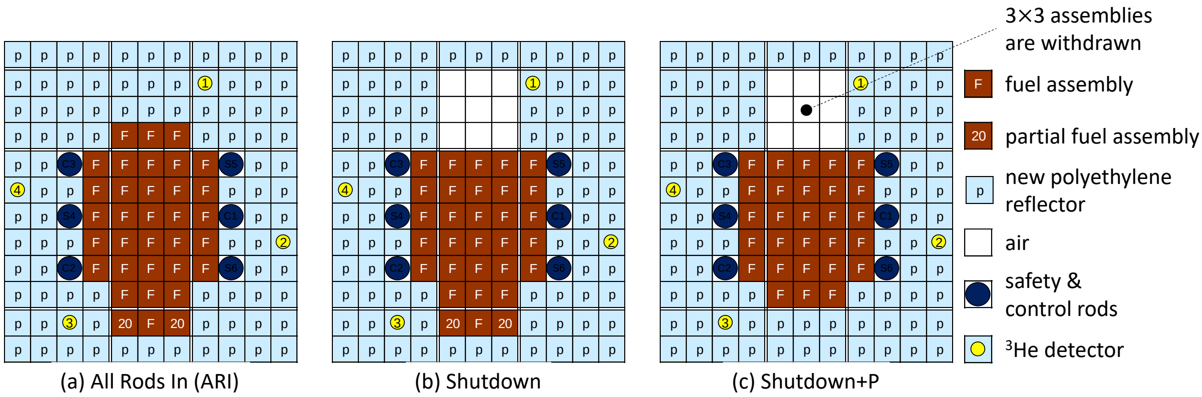

Figure 5 Top view of experimental cores (A3/8"p36EU-NU)

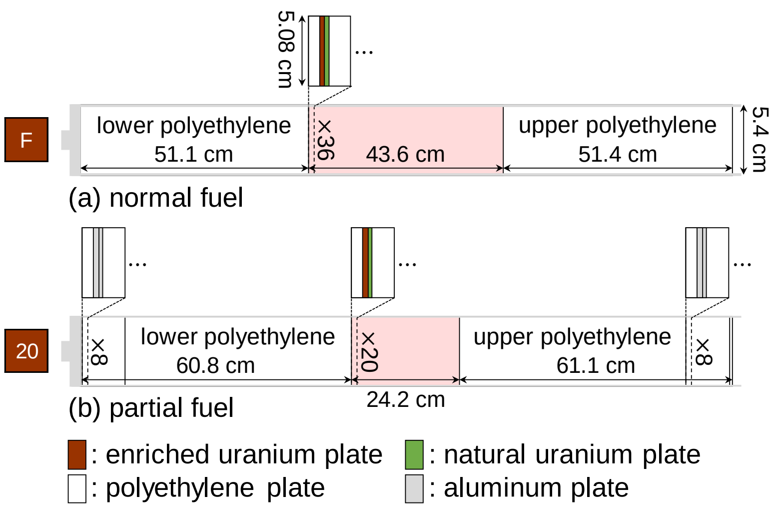

Figure 6 Fuel assemblies loaded in experimental core

Table 1 Numerical results of neutronics parameters for experimental cores

Case	k_{eff} (-)	β_{eff} (pcm)	Λ (μs)
(a) ARI	0.98120±0.00003†	776±6	39.65±0.03
(b) Shutdown	0.95118±0.00003	789±6	41.73±0.04
(c) Shutdown+P	0.93589±0.00003	794±6	42.15±0.04

† : 1σ statistical error

In this experiment, four ^{3}He detectors (#1–4) were placed at the axial center positions of the ex-core reflector assemblies. Using these detectors with a list-mode data acquisition system, the time-series data of neutron counts were successively measured. In Cases (a)–(c), the reactor noise was measured without any external neutron source such as an Am-Be or Cf source. In other words, the measurement was carried out using only the inherent neutron source, which mainly consists of the spontaneous fission of ^{238}U and (α,n) reactions of ^{27}Al owing to the α-decay of uranium isotopes [30]. To increase the neutron count rate, all the time-series data using detectors #1–4 were summed for the reactor noise analysis. Thereby, the neutron count rates $R = C_{\mathrm{ave}}(T)/T$ for Cases (a)–(c) were 74.12 ± 0.14, 29.98 ± 0.04, and 21.13 ± 0.03 (count/s), respectively.

The measurement times of the reactor noises were approximately 139.4 min, 975.0 min, and 933.5 min for Cases (a)–(c), respectively. It should be noted that Case (a) was measured during operation; thus, the measurement time was shorter than those in the shutdown states of Cases (b) and (c). Using the recursive bunching method, the variations in $\mathcal{Y}_n(kT_0)$, $\frac{\mathcal{Y}_3(kT_0)}{(Y(kT_0))^2}$, and $\frac{\mathcal{Y}_4(kT_0)}{(Y(kT_0))^3}$ were evaluated for each measurement, where $T_0 = 10^{-4}$ (s) and $M = 1024$, and the total number of count data N_0 were approximately 8.363×10^7, 5.850×10^8, and 5.601×10^8, respectively. To estimate the statistical errors of $\mathcal{Y}_n(kT_0)$, $\frac{\mathcal{Y}_3(kT_0)}{(Y(kT_0))^2}$, and $\frac{\mathcal{Y}_4(kT_0)}{(Y(kT_0))^3}$, the 95% bootstrap confidence intervals were also calculated using the moving block bootstrap method with $B = 1000$. Using the Feynman-α method [8,10,11] for the measured $Y(T)$, the prompt neutron decay constants α for Cases (a)–(c) were preliminarily estimated as 684.1 ± 3.5, 1307.4 ± 4.0, and 1618.5 ± 6.5 (1/s), respectively.

5.2. Experimental results

Figure 7 presents the variations in the second- to fourth-order neutron correlation factors $Y(T)$, $\mathcal{Y}_3(T)$, and $\mathcal{Y}_4(T)$ with respect to the counting gate widths T. In Figure 7, the error bars indicate the 95% bootstrap confidence intervals for $Y(T)$, $\mathcal{Y}_3(T)$, and $\mathcal{Y}_4(T)$. As can be seen in Figure 7, it was confirmed that these values converge to the saturation values Y_∞, $\mathcal{Y}_{3,\infty}$, and $\mathcal{Y}_{4,\infty}$ as T becomes sufficiently large. As shown in Equations (43) and (45), the magnitudes of Y_∞, $\mathcal{Y}_{3,\infty}$, and $\mathcal{Y}_{4,\infty}$ are approximately inversely proportional to the second, third, and fourth power of the subcriticality $-\rho$, respectively. Thus, these saturation values decreased as $-\rho$ deepened.

Figure 8 presents the variation in the ratios of $\frac{\mathcal{Y}_3(T)}{(Y(T))^2}$ and $\frac{\mathcal{Y}_4(T)}{(Y(T))^3}$ with the 95% bootstrap confidence intervals. In addition, Figure 9 presents the correlation matrices of the ratios between different counting gate widths T. As can be seen from the correlation matrices, there are strong correlations owing to the bunching method. These correlations decreased as the difference between kT_0 and $k'T_0$ increased, and as the subcriticality deepened.

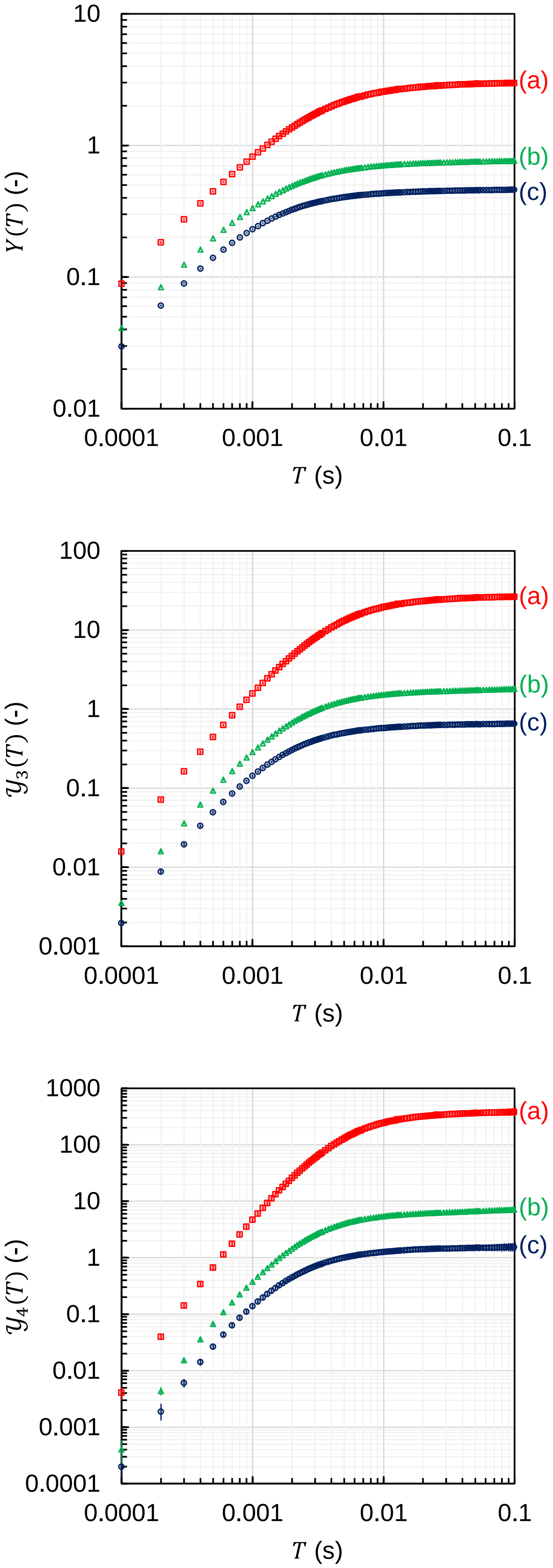

Figure 7 Experimental results of variations in $\boldsymbol{Y(T)}$, $\boldsymbol{\mathcal{Y}_3(T)}$, and $\boldsymbol{\mathcal{Y}_4(T)}$

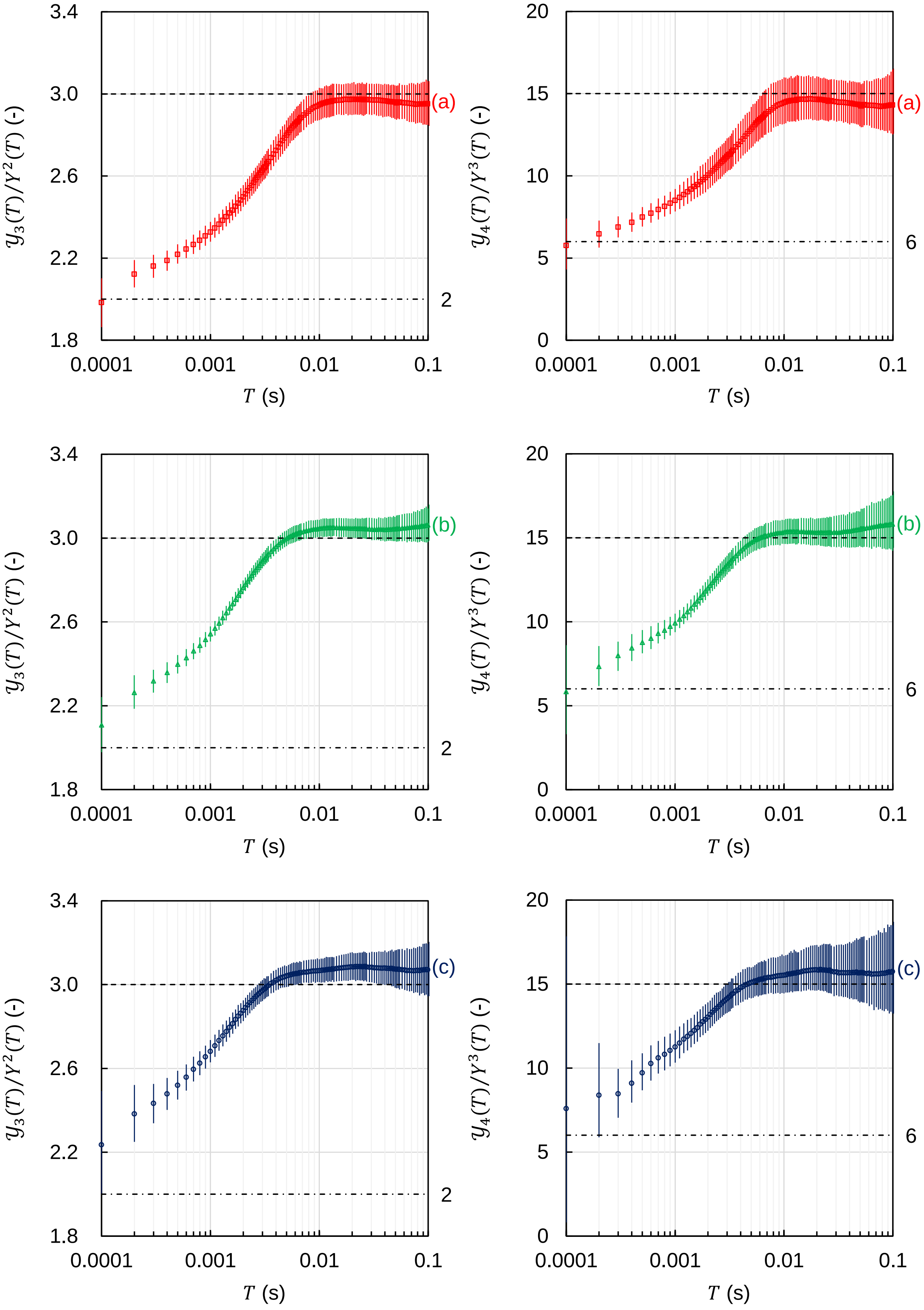

Figure 8 Experimental results of variations in $\mathcal{Y}_3(T)/(Y(T))^2$ and $\mathcal{Y}_4(T)/(Y(T))^3$

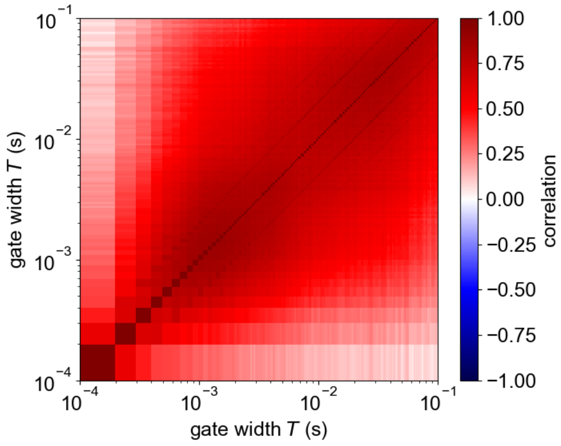

Case (a) $\mathcal{Y}_3(T)/\left(Y(T)\right)^2$

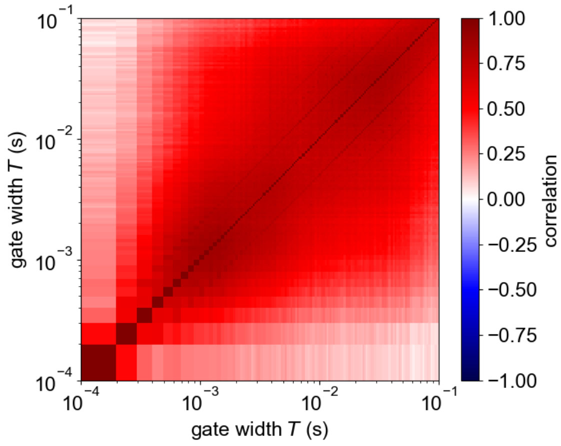

Case (a) $\mathcal{Y}_4(T)/\left(Y(T)\right)^3$

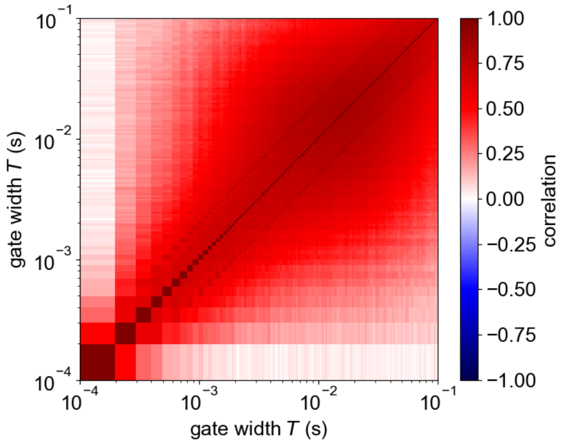

Case (b) $\mathcal{Y}_3(T)/\left(Y(T)\right)^2$

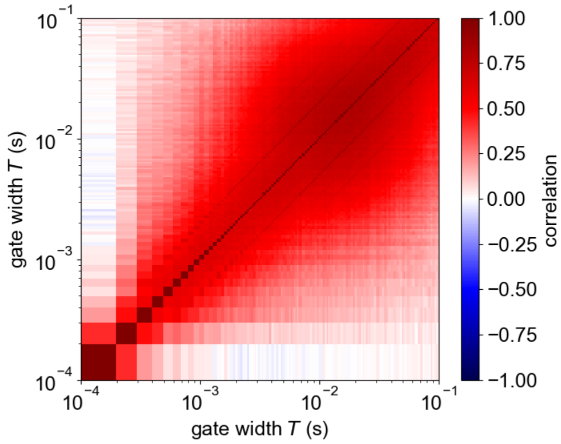

Case (b) $\mathcal{Y}_4(T)/\left(Y(T)\right)^3$

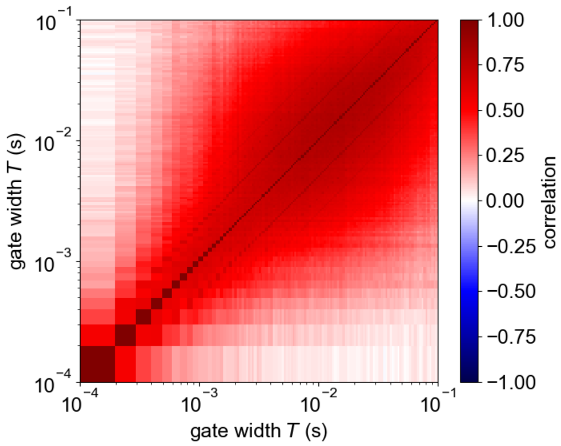

Case (c) $\mathcal{Y}_3(T)/\left(Y(T)\right)^2$

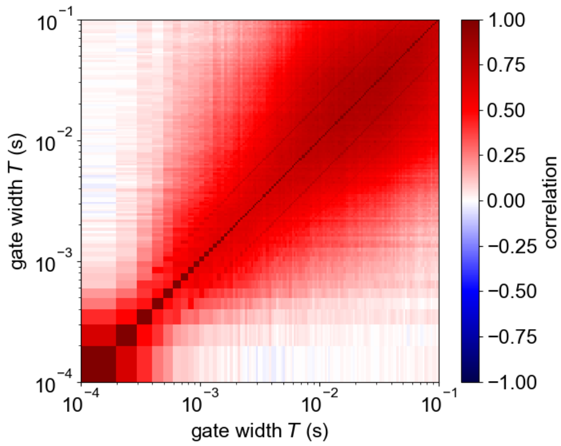

Case (c) $\mathcal{Y}_4(T)/\left(Y(T)\right)^3$

Figure 9 Experimental results of correlation matrices for $\boldsymbol{\mathcal{Y}_3(T)/\left(Y(T)\right)^2}$ and $\boldsymbol{\mathcal{Y}_4(T)/\left(Y(T)\right)^3}$

5.3. Discussion

As shown in Figure 8, $\frac{\mathcal{Y}_3(T)}{(Y(T))^2}$ and $\frac{\mathcal{Y}_4(T)}{(Y(T))^3}$ converge to the saturation values $\mathcal{Y}_{3,\infty}/Y_\infty^2$ and $\mathcal{Y}_{4,\infty}/Y_\infty^3$, as the gate width T (or the dimensionless quantity αT) becomes sufficiently large. If T is approximately larger than $10/\alpha \approx 0.01$ (s), the ratios appear constant, although there are statistical fluctuations. The 95% bootstrap confidence intervals of $\frac{\mathcal{Y}_3(T)}{(Y(T))^2}$ in Cases (a) and (b) included the unique combination number '3,' which was theoretically predicted by Equation (50). In Case (c), it should be noted that there were slight differences between $\frac{\mathcal{Y}_3(T)}{(Y(T))^2}$ and '3' when $0.01 < T < 0.03$ (s), whereas '3' was found within the 95% bootstrap confidence intervals when $T > 0.03$ (s). This observation confirms the relationships presented in Equation (48). For example, when $T = 0.02$ (s), $\left(\frac{\mathcal{Y}_3(T)}{(Y(T))^2} - 3\right) \approx 0.08 \pm 0.03$ (95% bootstrap confidence interval of $[0.02, 0.15]$), which approximately corresponds to the magnitude of $-\rho \approx 0.07$ in Case (c). If the measurement time of the reactor noise is increased by a factor of 4, the statistical significance of the difference between $\mathcal{Y}_{3,\infty}/Y_\infty^2$ and '3' can be detected, and $-\rho$ can be estimated more precisely using Equation (48). Similar to $\mathcal{Y}_{3,\infty}/Y_\infty^2$, it was confirmed that the 95% bootstrap confidence intervals of the saturated $\frac{\mathcal{Y}_4(T)}{(Y(T))^3}$ in Cases (a)–(c) included the unique combination number '15' of Equation (51). Consequently, Equations (50) and (51) were validated using the actual reactor noise measurement under the subcritical core, where $-\rho < 0.1$.

From Figure 8, it can be seen that $\frac{\mathcal{Y}_3(T)}{(Y(T))^2}$ and $\frac{\mathcal{Y}_4(T)}{(Y(T))^3}$ tended toward to '2' and '6' as T decreased to zero. This implies that the probability distribution of the neutron count $P(C, T)$ is sufficiently approximated by a negative binomial distribution under the condition of $Y_\infty(\alpha T)^2 \ll 1$ and $\alpha T \ll 1$, as clarified by previous research [33,34,35].

$$P(C,T) \approx \frac{\Gamma(C+r)}{C!\,\Gamma(r)}\left(\frac{m}{r+m}\right)^{C}\left(\frac{r}{r+m}\right)^{r}, \tag{59}$$

where $\Gamma(x)$ represents the Gamma function; m and r are the population parameters of the negative binomial distribution for the reproduction of $P(C,T)$. The probability generating function for Equation (59) can then be expressed as follows:

$$G(Z,T) \approx \left(\frac{r}{r+(1-Z)m}\right)^{r}. \tag{60}$$

Using Equations (1) and (59), $\langle C(T)\rangle$ and the second-, third-, and fourth-order neutron correlation factors can be obtained as

$$\langle C(T)\rangle = \left.\frac{\partial G}{\partial Z}\right|_{Z=1} = m, \tag{61}$$

$$Y(T) = \frac{1}{\langle C(T)\rangle}\frac{\partial^2}{\partial Z^2}\ln\big(G(Z,T)\big)\Big|_{Z=1} = \frac{m}{r}, \tag{62}$$

$$\mathcal{Y}_3(T) = \frac{1}{\langle C(T)\rangle}\frac{\partial^3}{\partial Z^3}\ln\big(G(Z,T)\big)\Big|_{Z=1} = 2\left(\frac{m}{r}\right)^2 = 2Y^2, \tag{63}$$

$$\mathcal{Y}_4(T) = \frac{1}{\langle C(T)\rangle}\frac{\partial^4}{\partial Z^4}\ln\big(G(Z,T)\big)\Big|_{Z=1} = 6\left(\frac{m}{r}\right)^3 = 6Y^3. \tag{64}$$

From Equations (62)–(64), it was confirmed that $\frac{\mathcal{Y}_3(T)}{(Y(T))^2} \approx 2$ and $\frac{\mathcal{Y}_4(T)}{(Y(T))^3} \approx 6$ if the negative binomial distribution approximation is applicable to $P(C,T)$. In particular, the ratios of '2' and '6' are approximately half of these unique combination numbers, '3' and '15.' Thus, it was suggested that approximate orders of magnitudes for $\mathcal{Y}_3(T)$ and $\mathcal{Y}_4(T)$ can be estimated from the second and third power of $Y(T)$ over the whole range of T.

6. Future study prospects

As shown in Figure 1, the unique combination numbers of $\mathcal{Y}_{n,\infty}/Y_{\infty}^{n-1}$ near the critical state can be inferred by the heuristic enumeration method for $n \geq 5$. Based on the heuristic method for the complete (unordered) binary tree, as shown in Figure 1, the unique combination numbers $b_n \equiv \mathcal{Y}_{n,\infty}/Y_{\infty}^{n-1}$ can be deduced using the double factorial [36]:

$$b_n \equiv \frac{\mathcal{Y}_{n,\infty}}{Y_{\infty}^{n-1}} = \prod_{k=1}^{n-1}(2k-1) = (2n-3)!!. \quad (65)$$

The sophisticated theoretical derivation for $\mathcal{Y}_{n,\infty}/Y_{\infty}^{n-1}$ for any system in the critical state is a topic of future work.

In Section 4, the virtual reactor noise measurement for the non-multiplication system with the ^{252}Cf source was verified with the aid of the Monte Carlo simulation. For the experimental validation, the actual measurement should be carried out, if possible. Hence, a high-efficiency neutron detection system is required to increase the magnitude of the neutron correlation factors $Y(T)$, $\mathcal{Y}_3(T)$, and $\mathcal{Y}_4(T)$.

In general, as the order of a neutron correlation factor $\mathcal{Y}_n(T)$ increases, the statistical error tends to increase. Hence, the experimental validation of the unique combination number for the significantly higher-order neutron correlation requires a longer measurement time of the reactor noise in a stable and unperturbed state such as the reactor shutdown state. From the experimental analysis conducted in this study, it can be concluded that $\mathcal{Y}_{3,\infty}/Y_{\infty}^{2}$ is relatively useful in comparison with $\mathcal{Y}_{4,\infty}/Y_{\infty}^{3}$ for the estimation of difference from the unique combination number, although the 95% confidence intervals of the experimental results were not sufficiently small. To reduce the statistical error of $\mathcal{Y}_{3,\infty}/Y_{\infty}^{2}$, the improvement of the detection efficiency and reduction of counting loss is necessary. Moreover, the measurement time should be increased depending on the subcriticality $-\rho$, because Equation (48) suggests that the difference between $\mathcal{Y}_{3,\infty}/Y_{\infty}^{2}$ and '3' increases as the subcriticality deepens.

In addition, the correlations of $\frac{\mathcal{Y}_3(T)}{(Y(T))^2}$ and $\frac{\mathcal{Y}_4(T)}{(Y(T))^3}$ between different counting gate widths T were significantly positive owing to the bunching method. Therefore, the saturation values in the fitting method or the averaging method should be carefully evaluated. In particular, if the correlations are neglected, the estimated standard errors for the saturation values may be underestimated. An advanced analysis methodology with consideration of the correlations should be conducted for the correct evaluation of the saturation values.

7. Conclusion

In this study, the fundamental physical properties of third- and fourth-order neutron correlation factors $\mathcal{Y}_3(T)$ and $\mathcal{Y}_4(T)$ in a source-driven subcritical system were theoretically derived. In particular, if the subcriticality $-\rho$ is approximately less than 0.1 (*dk/k*) =10000 (pcm), the saturation values of the ratios of $\mathcal{Y}_{3,\infty}/Y_\infty^2$ and $\mathcal{Y}_{4,\infty}/Y_\infty^3$ are almost equal to the unique combination numbers, '3' and '15,' independent of fissile materials and an external neutron source. The unique combination numbers, '3' and '15,' correspond to the total number of combinations for the trio- and quartet-detections, which have two and three two-forked branches, respectively, and are equal to the double factorial $(2n-3)!!$.

On the other hand, in the case of the non-multiplication system, $\mathcal{Y}_{3,\infty}/Y_\infty^2$ and $\mathcal{Y}_{4,\infty}/Y_\infty^3$ depend on the probability distribution of an external source $p_s(q)$. The ratios are significantly different from the unique combination numbers, '3' and '15.' Thus, the differences between $\mathcal{Y}_{3,\infty}/Y_\infty^2$ and '3' and between $\mathcal{Y}_{4,\infty}/Y_\infty^3$ and '15,' respectively, are useful information for the evaluation of whether the target system is in the near-critical state or not.

Using the moving block bootstrap method, the unique combination numbers, '3' and '15,' for the third- and fourth-order neutron correlation factors were validated using the actual zero-power reactor noise measurements carried out at KUCA. The moving block bootstrap method enabled the estimation of the statistical errors of $\frac{\mathcal{Y}_3(T)}{(Y(T))^2}$ and $\frac{\mathcal{Y}_4(T)}{(Y(T))^3}$, in addition to the correlation matrices between different gate widths T owing to the bunching method. Based on the experimental results, it was confirmed that approximate orders of magnitudes for $\mathcal{Y}_3(T)$ and $\mathcal{Y}_4(T)$ can be estimated using $\mathcal{Y}_3(T) \approx 3\big(Y(T)\big)^2$ and $\mathcal{Y}_4(T) \approx 15\big(Y(T)\big)^3$ over the whole range of T.

Furthermore, the results of experimental analysis reveal that the ratio of $\mathcal{Y}_{3,\infty}/Y_\infty^2$ is relatively useful in comparison with $\mathcal{Y}_{4,\infty}/Y_\infty^3$ for the estimation of the difference from the unique combination number, although the 95% confidence intervals of the present experimental results were not sufficiently small. The difference between $\mathcal{Y}_{3,\infty}/Y_\infty^2$ and ‘3’ is useful information for the statistical evaluation of whether the state is critical or subcritical, and for the determination of the absolute value of the subcriticality $-\rho$. The focus of future work will be directed toward the reduction of the statistical error of $\mathcal{Y}_{3,\infty}/Y_\infty^2$ and the development of an advanced analysis methodology for $\mathcal{Y}_{3,\infty}/Y_\infty^2$ with consideration of the correlations owing to the bunching method.

Acknowledgments

This work was carried out in part under the Visiting Researcher’s Program of the Research Reactor Institute, Kyoto University. The authors are grateful to all the technical staff at KUCA for their assistance during the experiment. This work was supported by the JSPS KAKENHI, Grant-in-Aid for Young Scientists (B) [Grant Numbers 15K18317 and 17K14909].

References

1. Hoogenboom JE, van der Sluijs AR. Neutron source strength determination for on-line reactivity measurements. Ann Nucl Energy. 1988;15(12):553–559.
2. Naing W, Tsuji M, Shimazu Y. Subcriticality measurement of pressurized water reactors during criticality approach using a digital reactivity meter. J Nucl Sci Technol. 2005;42(2): 145–152.
3. Tashiro S, Tojo M, Shimazu Y. Development of sub-criticality monitoring method during shutdown modes of nuclear power plants. Proc ICAPP 2017; 2017 Apr 24–28; Fukui and Kyoto, Japan.
4. Mukaiyama T, Nakano M, Mizoo N, *et al.* Reactivity measurement in a far-subcritical fast system (II); neutron source multiplication method. Ibaraki: Japan Atomic Energy Agency; 1975. JAERI-M 6067.
5. Naing W, Tsuji M, Shimazu Y. Subcriticality measurement of pressurized water reactors by the modified neutron source multiplication method. J Nucl Sci Technol. 2003;40(12):983–988.
6. Endo T, Yamamoto A, Yamane Y. Detected-neutron multiplication factor measured by neutron source multiplication method. Ann Nucl Energy. 2011;38(11):2417–2427.
7. Williams MMR. Random processes in nuclear reactors. Oxford (UK): Pergamon; 1974.
8. Feynman RP, de Hoffmann F, Serber R. Dispersion of the neutron emission in U-235 fission. J Nucl Energy. 1956;3(1–2):64–69.
9. Tonoike K, Yamamoto T, Watanabe S, *et al*. Real time a value measurement with Feynman-α method utilizing time series data acquisition on low enriched uranium system. J Nucl Sci Technol. 2004;41(2):177–182.
10. Endo T, Yamamoto A, Pyeon CH, *et al*. Statistical error estimation of the Feynman-α method using the bootstrap method. J Nucl Sci Technol. 2016;53(9):1447–1453.

11. Endo T, Yamamoto A. Comparison of theoretical formulae and bootstrap method for statistical error estimation of Feynman-α method. Ann Nucl Energy. 2019;124:606–615.
12. Orndoff JD. Prompt neutron periods of metal critical assemblies. Nucl Sci Eng. 1957;2(4):450–460.
13. Yamanaka M, Pyeon CH, Kim SH, *et al*. Effective delayed neutron fraction by Rossi-α method in accelerator-driven system experiments with 100 MeV protons at Kyoto University Critical Assembly. J Nucl Sci Technol. 2017;54(3):293–300.
14. Ricker CW, Hanauer SH, Mann ER. Measurement of reactor fluctuation spectra and subcritical reactivity. Nucl Sci Eng. 1968;33(1):56–64.
15. Sakon A, Hashimoto K, Sugiyama W, *et al*. Power spectral analysis for a thermal subcritical reactor system driven by a pulsed 14 MeV neutron source. J Nucl Sci Technol. 2013;50(5):481–492.
16. Furuhashi A, Izumi A. Third moment of the number of neutrons detected in short time intervals. J Nucl Sci Technol, 1968;5(2):48–59.
17. Dragt JB. Threefold correlations and third order moments in reactor noise. Nukleonik, 1967;10(1):7–13.
18. Endo T, Yamane, Y, Yamamoto A., Space and energy dependent theoretical formula for the third order neutron correlation technique. Ann Nucl Energy. 2006;33(6):521–537.
19. Kitamura Y, Endo T. Yamane Y, *et al*. Absolute measurement of the subcriticality by using the third order moment of the number of neutrons detected. Proc PHYSOR 2002; 2002 Oct 7–10; Seoul, Korea.
20. Humbert P. Third order time correlation method applied to SILENE absolute criticality measurements. Proc PHYSOR 2010; 2010 May 9–14; Pittsburgh, USA.
21. Efron B. Bootstrap methods: another look at the Jackknife. Ann Stat. 1979;7(1):1–26.
22. Künsch HR. The Jackknife and the bootstrap for general stationary observations. Ann Stat. 1989;17(3), 1217–1241.

23. Humbert P. Simulation and analysis of list mode measurements on SILENE reactor. J Comp Theor Trans. 2018. DOI: 10.1080/23324309.2018.1477802
24. Endo T, Kitamura Y, Yamane Y. Absolute measurement of the subcriticality based on the third order neutron correlation in consideration of the finite nature of neutron counts data. Proc ICNC2003; 2003 Oct 20–24; Tokai, Japan.
25. Cramér H. Mathematical methods of statistics. Princeton (NJ): Princeton University Press; 1946.
26. Endo T, Yamane Y, Yamamoto A. Derivation of theoretical formula for the third order neutron correlation technique by using importance function. Ann Nucl Energy. 2006;33(10):857–868.
27. Endo T, Yamamoto A, Yamane Y. Development of deterministic code based on the discrete ordinates method for the third-order neutron correlation technique. Ann Nucl Energy 2008;35(5):927–936.
28. Gwin R, Spencer RR, Ingle RW. Measurements of the energy dependence of prompt neutron emission from ^{233}U, ^{235}U, ^{239}Pu, and ^{241}Pu for E_n = 0.005 to 10 eV relative to emission from spontaneous fission of ^{252}Cf. Nucl Sci Eng. 1984;87(4):381–404.
29. Maeno K, Endo T, Yamamoto A. Evaluation of the n/γ discrimination performance of the neutron detector with Eu doped TRUST-LiCaAlF6. Proc ICAPP 2017; 2017 Apr 24–28; Fukui and Kyoto, Japan.
30. Shiozawa T, Endo T, Yamamoto A, *et al*. Investigation on subcriticality measurement using inherent neutron source in nuclear fuel. Ibaraki: Japan Atomic Energy Agency; 2015. JAEA-Conf 2014-003.
31. Werner CJ (editor). MCNP User’s manual code version 6.2. Los Alamos (NM): Los Alamos National Laboratory; 2017. LA-UR-17-29981.
32. Shibata K, Iwamoto O, Nakagawa T, *et al*. JENDL-4.0: A new library for nuclear science and engineering. J Nucl Sci Technol. 2011;48(1):1–30.

33. Szeless A, Ruby L. Reactor noise parameters by the maximum likelihood method. Trans Am Nucl Soc. 1969;12:739–740.
34. Szeless A, Ruby L. The exact probability distribution of reactor neutron noise. Nucl Sci Eng. 1971;45(1):7–13.
35. Nakajima K, Hohara S, Sakon A, *et al*. Experimental investigation on probability distribution of neutron counts in a nuclear reactor. Proc PHYSOR 2018; 2018 Apr 22–26; Cancun, Mexico.
36. Stanley RP. Enumerative combinatorics: volume 2. Cambridge (UK): Cambridge University Press; 1999. Chapter 5, Trees and the composition of generating functions; p. 1–158.